García-Marín, J. (2020) Computational insight into the selective allosteric inhibition for PTP1B versus TCPTP: a molecular modelling study, Journal of Biomolecular Structure and Dynamics, 39(15), pp. 5399-5410.

Computational insight into the Selective Allosteric Inhibition for PTP1B versus TCPTP: A Molecular Modelling Study

Garcia-Marin J[a,b,c,*]

[a]*Departamento de Química Orgánica y Química Inorgánica, Facultad de Farmacia, Universidad de Alcalá, 28805 Alcalá de Henares, Spain*

[b]*Instituto Ramón y Cajal de Investigación Sanitaria (IRYCIS), Ctra Colmenar Viejo, km 9100, 28034 Madrid, Spain*

[c]*Instituto de Investigación Química Andrés M. del Río, Facultad de Farmacia, Universidad de Alcalá, 28805, Alcalá de Henares, Spain.*

javier.garciamarin@uah.es

Corresponding Author: Garcia-Marin, Javier. Departamento de Química Orgánica y Química Inorgánica, Facultad de Farmacia, Universidad de Alcalá, 28805 Alcalá de Henares, Spain. javier.garciamarin@uah.es

Abstract

All over the world, diabetes mellitus type 2 has spread as a problematic pandemic. Despite currently available treatments, approved drugs still show undesirable side effects and loss of efficacy or target symptoms instead of causes. Protein tyrosine phosphatase 1B (PTP1B), since its discovery, has emerged as a very promising target against this disease. Although the information regarding the enzyme is immense, little is known about the selectivity between this enzyme and its closest homologue, lymphocyte T tyrosine phosphatase (TCPTP), which is responsible for complicated side effects. In this study, on the basis of different computational approaches, we are able to highlight the importance of a phenylalanine residue located in PTP1B, but not in TCPTP, as a crucial hotspot that

causes selectivity and stability for the whole ligand bound system. These results not only allow to explain the selectivity determinants of PTP1B but also provide a useful guide for the design of new allosteric inhibitors.

Keywords Diabetes Mellitus, PTP1B, TCPTP, molecular dynamics.

Abbreviations

T2DM: diabetes mellitus type 2, PTP1B: protein tyrosine phosphatase 1B, TCPTP: T-cell protein tyrosine phosphatase, MD: molecular dynamics, ns: nanosecond, fs: femtosecond, RMSD: root-mean-square deviation, RMSF: root-mean-square fluctuation.

Introduction

Nowadays, diabetes mellitus type 2 (T2DM) has become a worldwide health problem. In fact, the number of people with T2DM has significantly increased over the last decade, and about 1 in 11 adults suffer from this disease (Zheng, Ley, & Hu, 2018). This condition is characterised by peripheral insulin resistance in tissues and by a pancreatic β-cell dysfunction (Chatterjee, Khunti, & Davies, 2017). Consequently, the search for new drugs to combat this disorder has become a hotspot for pharmaceutical and academic research groups. In the last years, new drugs, including SLGT-2 inhibitors, DPP-IV inhibitors and GLP-1 agonists, have been introduced in the market. However, laboratories continue to study novel therapeutic approaches to overcome the side effects or address the lack of efficiency of such treatments.

In the late 80s, Tonks et al discovered a very promising phosphatase, PTP1B, which was validated, few years later, as a therapeutic target for T2DM treatment (Elchebly et al.,

1999; N K Tonks, C D Diltz, & E H Fischer, 1988). Moreover, PTP1B is associated with T2DM via the leptin signalling cascade as a negative leptin regulator; hence, PTP1B is also of interest as a therapeutic target for anti-obesity drugs (Bence et al., 2006; Johnson, Ermolieff, & Jirousek, 2002). Unfortunately, active-site PTP1B inhibitors failed in preclinical phase because the conserved active-site requires charged molecules, such as phosphotyrosine mimetics, also known as the first generation of inhibitors, which compromise the ADME properties of these putative drug candidates. Therefore, no active-site inhibitors reached phase I clinical trials. In fact, PTP1B was considered as a challenge for medicinal chemists. Consequently, the perspectives for the PTP1B inhibition by small molecules remained uncertain.

Allosteric inhibition is a very advantageous strategy, especially in the case of PTP1B, since it could provide more selective drugs with enhanced drug-like properties (Kumar, A. P., Nguyen, Verma, & Lukman, 2018; Shen et al., 2004). Moreover, allosteric sites are a new source of binding sites for undruggable targets and also can provide the opportunity of regulating drug effects (Abdel-Magid, 2015) or modulation of the protein activity rather than eliminating it (Nussinov & Tsai, 2013). In fact, for PTP1B, several non-competitive and allosteric inhibitors, including a squalene derivative called trodusquemine (ClinicalTrials.gov Identifier: NCT00806338) or the candidate JTT-551 (Ito, Fukuda, Sakata, Morinaga, & Ohta, 2014), have reached clinical trials.

In 2004, Wiesmann reported the first-in-class allosteric inhibitors of PTP1B and their crystal structures bound to the protein (Figure 1). These ligands bind to a non-explored region previously, located about 20 Å away from the catalytic site. The binding mechanism starts with the opening of a cavity between α-3, α-6 and α-7 helix and leads

to a partial unfolding of the latter one, located in the *C*-terminal part of the enzyme. To simplify, the allosteric network produces a series of motions in the secondary structure that eventually blocks the catalytic WPD loop in its open state conformation (Cui, W. et al., 2013; Li et al., 2014). These structures are necessary for understanding allosteric inhibition in PTP1B, and so, several molecular modelling studies have been conducted to rationalise structural motions (Li et al., 2014; Olmez & Alakent, 2011a) or rationalise affinities (Bharatham, Bharatham, Kwon, & Lee, 2008; Cui, W. et al., 2013; Yangmee Kim, Jee-Young Lee, Ki-Woong Jung, & Eun-Rhan Woo, 2008).

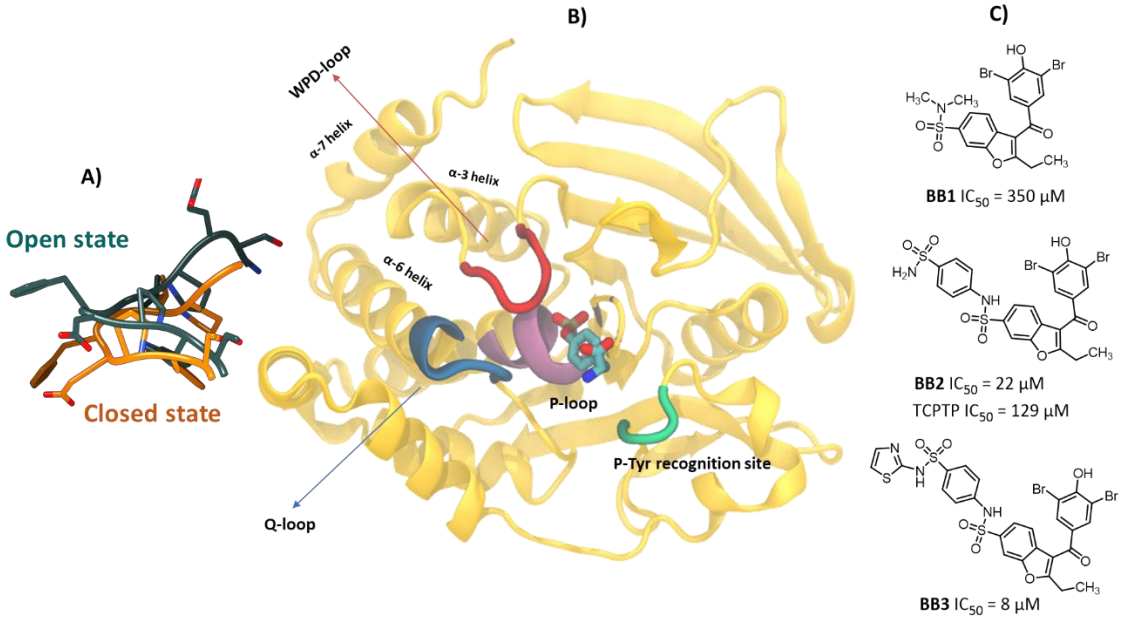

Fig 1. A) Open and closed states for WPD-loop in PTP1B (PDB: 1T4J and 2NTA respectively). B) Full structure of PTP1B (PDB:1PTY, (Puius et al., 1997)). C) The three allosteric inhibitors reported by Wiesmann (Wiesmann et al., 2004).

Conformational motions are of great importance for enzyme catalysis (Garuti & Bottegoni, M. Roberti and G.; Kulkarni et al., 2017) and selectivity (Colombano et al., 2019; Joyce et al., 2008) and should be considered during the drug design process

(Huggins, Sherman, & Tidor, 2012). For PTP1B, selectivity has been shown to be essential because, like kinases, phosphatases share a quite conserved catalytic site and the selective inhibition is better reached by targeting off-site structural motifs. Indeed, TCPTP shares more than 75% homology with PTP1B at the catalytic site, and the inhibition of the former causes severe undesirable effects (You-Ten et al., 1997). However, to the best of our knowledge, so far, no computational reports have shed light on the observed selectivity of allosteric inhibitors for PTP1B. Only the presence of a Cys278 residue in TCPTP, rather than a Phe280 residue in PTP1B, at the allosteric pocket of both enzymes has been suggested as the probable cause of the observed selectivity (Shinde & Sobhia, 2013; Wiesmann et al., 2004). Here, we shed new light on the observed selective inhibition for PTP1B versus TCPTP of benzbromarone-based allosteric inhibitor BB2 reported by Wiesmann. To this aim, computational methods such as classical all-atoms molecular dynamics (MD) and end-point free energy methods were applied.

Material and Methods

Modelling of PTP1B and TCPTP complexes

Homology model techniques were used because the allosteric sites of PTP1B and TCPTP are not completely solved in the presence of an inhibitor and in its open state. The allosteric site was modelled as described previously (Shinde & Sobhia, 2013; Shinde, Kumar, Eqbal, & Sobhia, 2018). Briefly, the crystal structure of PTP1B (2F6F), together with 1T48, was used, both with the WPD loop in the open conformation. To construct the TCPTP complexes, the complete sequence was retrieved from Uniprot (P17706) and aligned to the crystal structure sequences of 1L8K and 1T48, used as templates to build missed residues corresponding to the α6-α7 loop and α7 helix. Homology modelling was

carried out using MODELLER 9.22 (Šali & Blundell, 1993) and its graphic user interface for Chimera 1.13 (Pettersen et al., 2004).

In both cases, the benzbromarone inhibitor BB2 was included in the template PDB as a conformational constraint to build the final models. Thereafter, using PyMol (The PyMOL Molecular Graphics System, Version 1.8 Schrödinger, LLC), the coordinates for the allosteric inhibitor were transferred from 1T48 to the new models, BB2–PTP1B and BB2–TCPTP. Protonation states of the whole protein were assigned using H ++ server (http://biophysics.cs.vt.edu/H++).

Molecular dynamics

For ligand parametrisation, GAFF forcefield (Wang, J., Wolf, Caldwell, Kollman, & Case, 2004) was used in combination with AM1-BCC partial atom charges generated with Antechamber, as implemented in AmberTools 16 (Case et al., 2005). Protein atoms were described using Amber ff14SB (Maier et al., 2015) and the TIP3 (Jorgensen, Chandrasekhar, Madura, Impey, & Klein, 1983) water model. All complexes were immersed in a cubic water box extended 12.0 Å from the solute, and then, 5 and 3 sodium ions were added to PTP1B and TCPTP systems, respectively, until electroneutrality was reached. For long-range electrostatic interactions, the particle mesh Ewald method was used, whereas non-bonded interactions were truncated at 10.0 Å. All bonds involving hydrogen were constrained using SHAKE algorithm (van Gunsteren & Berendsen, 1977). All-atoms MD simulations began in three steps using Sander module after a previous minimisation of hydrogens, water molecules and protein atoms. First, the system was gradually heated up to 300 K using a time step of 2.0 fs over a period of 50 ps, applying positional restrains to the protein backbone atoms (harmonic constant of 100 $kcal \cdot mol^{-1} Å^{-2}$). Then, 50 ps of NVT simulation was conducted to release the restrains, and it was

followed by systems equilibration in the NVT ensemble for 100 ps using Lanvegian temperature control. Production was performed using NAMD 2.12 (Phillips et al., 2005) in a GPU NVIDIA for CUDA acceleration. Four 50 ns simulations of MD production were generated in the NPT ensemble using Nosé–Hoover Langevin piston (Nosé, 1984) pressure control.

Analysis

To assess root-mean-square deviation (RMSD), root-mean-square fluctuation (RMSF), principal component analysis (PCA) and distances, the produced trajectories were analysed by Jupyter Notebooks using MDTraj (McGibbon et al., 2015). All measures were in reference to the starting geometries generated for PTP1B and TCPTP complexes. Contacts between protein residues and ligand were calculated with Python package ContactMap (https://contact-map.readthedocs.io/en/latest/). Hydrogen bond analysis was conducted with the HBond plugin implemented in VMD (Humphrey, Dalke, & Schulten, 1996). For the analysis, hydrogen bonds were defined by acceptor–donor atom distances shorter than 3.5 Å and acceptor–H–donor angles larger than 120°. Trajectory visualisation was conducted with VMD and Chimera Software packages.

Statistical analysis of RMSD and distances data shown are mean (± SD) values. Significance between data series was determined via t-test or ANOVA using GraphPad Prism version 7.00 for Windows (San Diego, CA). A p value < 0.05 was considered statistically significant.

Free energy calculations

For ligand affinity, free energy calculations were performed using MMPBSA.py (Miller et al., 2012) module implemented in Ambertools 16. The molecular mechanics Poisson–Boltzmann surface area (MMPBSA) is based on the analysis of MD trajectories using a continuum solvent approach. A total of 150 snapshots were taken from the last 25 ns of the ligand complexes trajectories to apply MMPBSA calculations to the equilibrated structure and to obtain significant results (Genheden & Ryde, 2010). All calculations used a solute internal dielectric constant of 1 and an external dielectric constant of 80. Finally, per-residue free energy decomposition was studied using the Python-based plugin CHEWD (Raza et al., 2019). This tool also helps to easily visualise and to understand the differences in per-residue energy contribution with a user-friendly and interactive residue colouring post-processing.

Results and Discussion

Structural stability and flexibility of simulated complexes

To study the behaviour of BB2 complexed to PTP1B and TCPTP in solution, proteins were simulated both in the apo and ligand bound forms, in the presence of explicit water molecules as solvent. The starting geometry was the inactive, open conformation of the WPD loop. Homology modelling techniques were used because the α7 helix was not completely solved in the presence of an allosteric inhibitor (1T49). Then, using Ramachandran plots, all systems were visually inspected and evaluated prior to its simulation (see supporting information).

In total, four 50 ns MD simulations were performed and named as apo PTP1B and apo TCPTP, for full enzymes, and BB2–PTP1B and BB2–TCPTP, for full ligand complexes. First, structural stability was assessed by computing the RMSD for backbone atoms of the whole protein in reference to the starting frame of the simulation (Fig. 2).

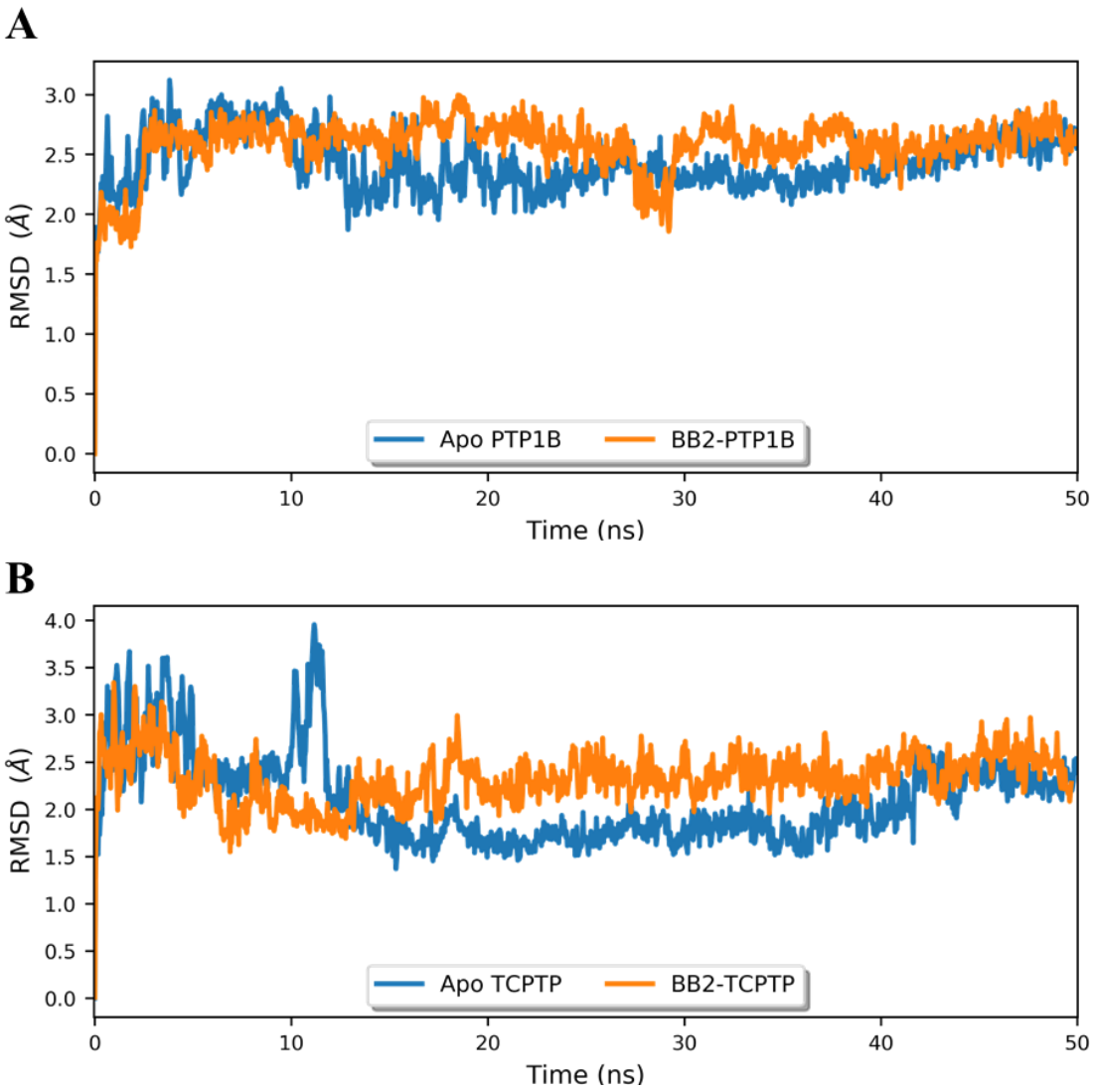

Fig 2. RMSD profiles: A) apo PTP1B (blue) and BB2–PTP1B (orange); B) apo TCPTP (blue) and BB2–TCPTP (orange).

Apo PTP1B tended to reach the equilibrium after ~12 ns of simulation in the isobaric–isothermal (NPT) ensemble (panel A), whereas apo TCPTP reached the equilibrium after ~15 ns (panel B). It is worth noting that in the simulation, apo PTP1B showed significantly less fluctuations and higher stability compared with its homologue, apo TCPTP, with mean RMSD of 2.396 and 2.7 Å ($p = 0.0001$), respectively. Moreover, since the partially uncoiled α7 helix presented a high motion along with the four simulations, high RMSD values were expected. Ligand binding has resulted in a slight increment in the RMSD values for BB2–PTP1B compared with apo PTP1B, although the complex reached equilibrium more quickly (~5 ns). A similar scenario occurred in the BB2–TCPTP system where the RMSD values showed a slightly higher increment than that observed in BB2–PTP1B, reflecting the increased flexibility of the whole protein, as suggested by the change in the mean RMSD value from 2.70 to 2.84 Å ($p = 0.0042$) (panel B). Subsequently, both complexes remained stable throughout the rest of the simulation time.

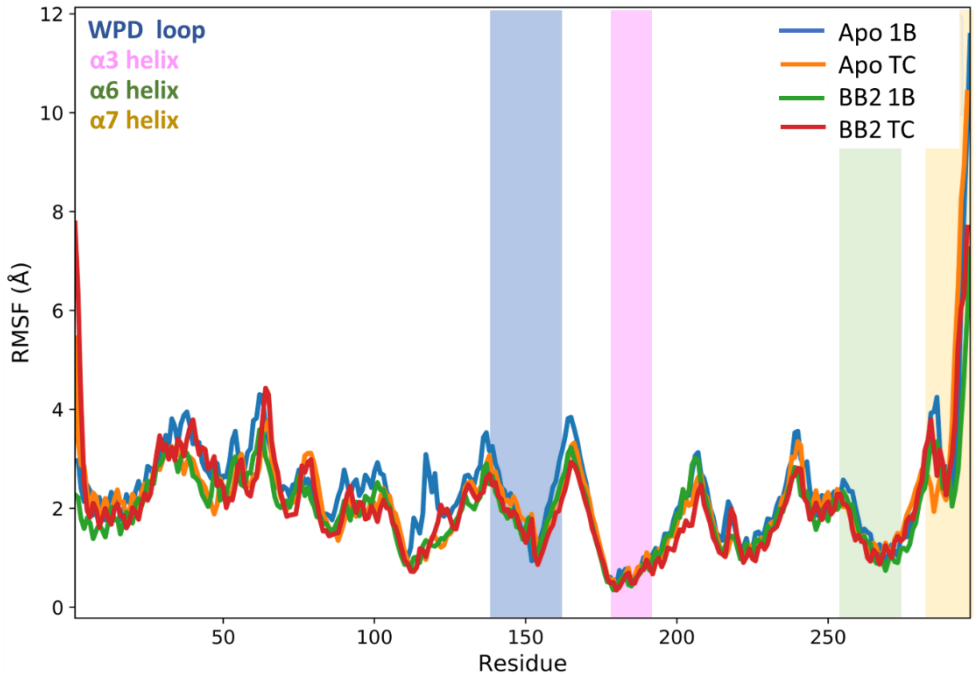

Fig. 3. Plot analysis of the Cα RMSF for apo proteins and BB2 complexes.

The RMSF profiles for full complexes and apo proteins were monitored to get a more detailed information about its flexibility (Fig. 3).

During the simulations, the analysis of the Cα RMSF values also showed both plastic and stable parts of the protein. As previously described, regions with higher RMSF corresponded to those of the *C*-termini for both phosphatases (Jin, Yu, & Huang, 2016). The highest peaks corresponded to residues present in the α7 helix, which was partially disordered in both structures. A high RMSF is also observed in the *N*-terminus for apo TCPTP with values of 6–8 Å, making this system more flexible than apo PTP1B. The WPD loop was tended to present smaller fluctuations near 3.0–4.0 Å, whereas no very significant fluctuations were observed for other important secondary structure elements, including helixes α3 and α6. Despite this, it could be observed that slightly higher RMSF values were found for apo systems than in holo complexes. This may suggest the ability of the inhibitor to stabilise the open conformation of the catalytic WPD loop. Moreover, the overall conformation of the catalytic domain is very similar to that of the crystal structure. This was checked by the comparison with B factors present in the crystal structure 1T49 and 1L8K; meaning, both apo proteins show similar catalytic abilities for competitive inhibitors. Furthermore, it was observed that BB2–TCPTP complex presented slightly lower RMSF values than apo TCPTP. These results are in good agreement with previous studies that relate a partial destabilisation of the α7 helix upon ligand binding inside the allosteric pocket (Cui, W. et al., 2013; Wiesmann et al., 2004).

Analysis of key interactions

To examine differences and changes in the binding mode and recognition process of these tyrosine phosphatases towards BB2, RMSD measurements were performed for some key components of the allosteric pocket. During the simulation time, it is clearly observed that, for the BB2–PTP1B complex, the initial binding mode of the inhibitor is well maintained during the trajectory to accommodate the ligand inside the flexible pocket (Fig. 4). However, BB2–TCPTP presented a different scenario. RMSD values, obtained from the homology model, showed how the initial binding mode had random fluctuations inside this cavity (Fig 4). The ligand slightly shifted out from the initial binding site during the first 3 ns of simulation where the benzofuran core flipped to a vertical position and then returned to the starting planar position. Additionally, a displacement of the α7 helix took place at the end of the simulation to establish a partially displaced parallel π–π stacking with the dibromophenole ring of BB2. Nonetheless, hydrogen bonding pattern with $Asn193_{PTP1B}$/$Asn194_{TCPTP}$ and $Glu276_{PTP1B}$/$Glu274_{TCPTP}$ within the allosteric site tended to maintain the overall binding mode, only very slight fluctuations were observed.

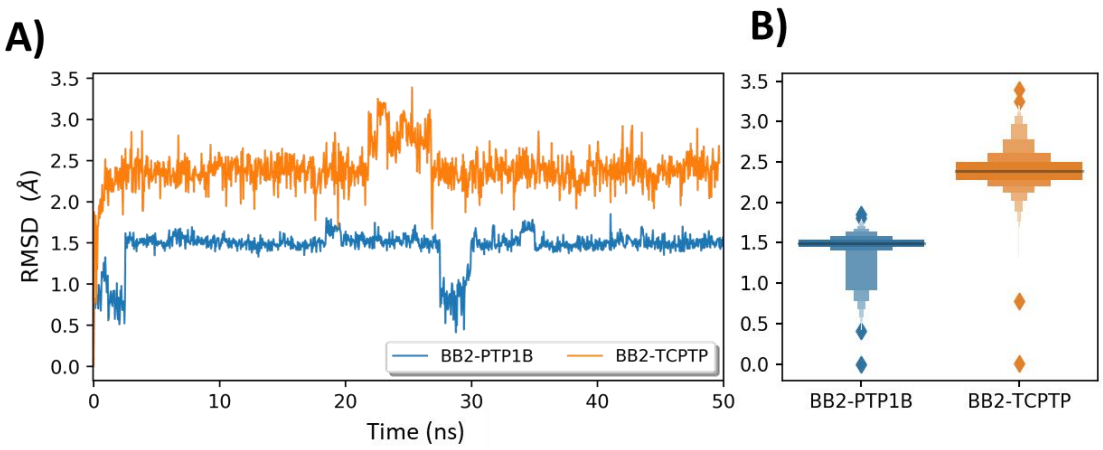

Fig. 4. A) RMSD for ligand atoms of complexes BB2–PTP1B and BB2–TCPTP at the allosteric pocket. B) Box-plot with RMSD values distribution from A).

Protein–ligand complexes are usually stabilised by the presence of directional

intermolecular interactions including hydrogen bonds, salt bridges or even covalent bonds. Subsequently, the hydrogen bond network of BB2 bound to the allosteric pocket was monitored during the simulation to try to rationalise the differences observed in the stability of both systems. An initial analysis showed a slightly more populated hydrogen bond network for BB2–PTP1B complex than for the BB2–TCPTP complex (Fig. 5). This is well illustrated by the prevalence of hydrogen bonds across the simulation (Table 1).

Table 1. Hydrogen bonding interactions for BB2 at the allosteric site of PTP1B (1B) and TCPTP (TC).

Residue PTP1B/TCPTP	Residue atom	Atom (BB2)	Simulation time (%)		Average distance (Å)	
			BB2–1B	BB2–TC	BB2–1B	BB2–TC
Glu 276/274	OE2	NO1	79.36	88.9	2.89	3.2
Trp 291/289	OE2	O19	6.84	2.98	3.1	3.5
Asn 193/194	ND2	O19	70.4	51.65	2.05	2.1

Overall, the average number of hydrogen bonds during 50 ns MD simulations is slightly higher in the BB2–PTP1B complex. Ligand BB2 establishes hydrogen bonds with Glu, Asn and Trp residues present in the allosteric cavity of both proteins during our simulations. The most stable hydrogen bond is formed between the NH of the sulphonamide group and the carboxylate group of a Glu residue present in both enzymes

(Glu276$_{PTP1B}$/Glu274$_{TCPTP}$) that can bind to BB2 through its two oxygen atoms, OE1 and OE2. Although there is a slightly higher prevalence for the BB2–TCPTP complex (88.9% vs 79.36%), a better mean distance is observed for the case of BB2–PTP1B (2.89 vs 3.2 Å). This could be explained, as can be observed in terms of RMSD, by the apparently lower fluctuations within the allosteric cavity for BB2–PTP1B than those for BB2–TCPTP (Fig. 4). Moreover, the carbonyl group of BB2 is hydrogen bonded to the NH_2 of the carboxamide group present in the Asn193$_{PTP1B}$/Asn194$_{TCPTP}$ residue. This interaction presents a better occurrence for the PTP1B complex than for the TCPTP complex (70.4% vs 51.65%). The eventual loss of this interactions seemed to be compensated for the π-π stacking mediated by Phe280 inner the cavity of PTP1B allosteric site, while in the case of TCPTP is partially compensated for the rest of van der Waals interactions inside the pocket. Additionally, the NH group of Asn191$_{PTP1B}$/Asn189$_{TCPTP}$ can establish eventual electrostatic interactions with the oxygen atoms of the sulphonamide group in BB2, with lower prevalence for both systems but slightly higher in the case of the BB2–PTP1B complex. Furthermore, hydrogen bonding could be occasionally observed between the sulphonamide group and the carbonyl group of Ser285$_{PTP1B}$/Ser284$_{TCPTP}$ located in the α7 helix of both enzymes. All the interactions mentioned above are flexible during the simulations, but, overall, they seem to reflect a stronger binding of BB2 to the allosteric pocket of PTP1B as can be deduced by the numbers of hydrogen bonds established during the simulation (Fig. 5).

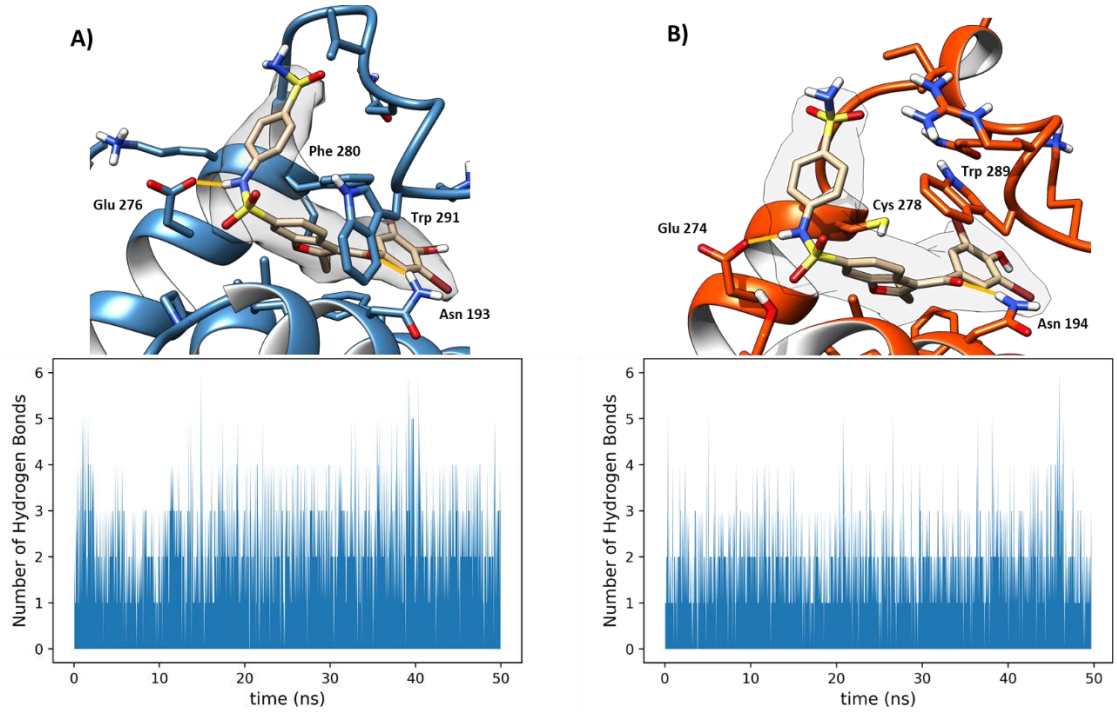

Fig. 5. Representative snapshot of the trajectory and number of hydrogen bond profiles between A) BB2 and PTP1B; B) BB2 and TCPTP.

In addition to the electrostatic interactions of BB2, the benzofuran core is placed in a hydrophobic pocket bordered by Leu192, Phe196, Phe280 and Trp291 in PTP1B and its homologue residues Leu193, Phe197, Cys278 and Trp289 in TCPTP. It is vital to recognise that there is a π–π stacking interaction through the benzofuran ring and of Phe280. This interaction presented an average distance of 2.89 Å across the simulation, reflecting its strong stability since the benzofuran core was kept stable inside the pocket. However, in the case of TCPTP, this position is substituted by Cys278. Consequently, only a weaker hydrophobic interaction is established in this complex. The main consequences are then the higher fluctuations observed during the visualisation of the simulation and the higher RMSD of the ligand. Evidences of the slightly higher fluctuations of the ligand inside the pocket can also be deduced by the data of ligand atom

occupancy. VolMap plugin allowed to observe a higher occupancy volume for BB2–TCPTP complex than BB2–PTP1B for a same contour level (Fig.5). Overall, it appears that there is a slight difference in how the enzymes respond to the same ligand and the outcome of the observed differences agree with the inhibitory effect of BB2 and its selectivity towards PTP1B in terms of IC_{50} (Fig.1).

Geometry analysis of the binding site

A more exhaustive analysis was performed for the structural components of the allosteric site because of the differences observed in the key interactions for both complexes. BB2 is placed in a cavity flanked by three alpha helixes. For this study, the previously described Karmerlyn criteria (Kamerlin, Rucker, & Boresch, 2007) were followed to study the next segments: residues 186–200, 264–281 and 287–295 were respectively selected for the study of α3, α6 and α7 helixes in PTP1B, and residues 185–199, 260–279 and 289-291, for partner helixes, respectively, in TCPTP. We also focused our attention to the WPD loop, which comprised residues 178–186 in TCPTP and 177–185 in PTP1B.

Allosteric inhibitors can stabilise a conformation associated with the open form of PTP1B (WPD loop open), which is catalytically inactive. This conformation is a response to an allosteric communication network between α7 helix and WPD loop. In its apo form, WPD loop switches between open and closed conformations (Cui, D. S., Lipchock, Brookner, & Loria, 2019; Li et al., 2014), whereas once the allosteric ligand is bound to the allosteric pocket, the WPD loop remains open. Subsequently, different RMSD were studied to acquire more insights into the dynamics of the WPD loop and allosteric helixes (Table 2). For the four systems, RMSD analysis in the WPD loop reveals higher values for the apo form. Higher RMSD values tend to match with a more mobile WPD loop, swinging

from an open to a closed state (Olmez & Alakent, 2011b). This is well illustrated in the case of BB2–PTP1B where RMSD is slightly lower, explaining the higher stability of the open state for this complex after ligand binding. RMSD lowers 0.36 Å in the case of PTP1B and only 0.14 Å for TCPTP ($p = 0.0001$), with standard deviation for the latter (0.46 Å) higher than that for the former (0.32 Å). As regards RMSD for allosteric helixes, there is a lowering for helixes α3 and α6 upon ligand binding to PTP1B, but this is not the case when ligand binds to TCPTP. Surprisingly, although they reached value is still significantly lower than that reached in BB2–PTP1B, a strong lowering in RMSD was observed for helix α7 in BB2–TCPTP. In brief, both proteins stabilise as a consequence of an overall lowering of the motions of the allosteric helixes and the WPD loop upon ligand binding. However, this stabilisation is lower but statistically significant ($p = 0.0027$) for BB2–TCPTP in terms of mean RMSD than for BB2–PTP1B, suggesting a weaker effect on the whole protein when BB2 binds to TCPTP.

Table 2. RMSD ± SD values for secondary structure elements in both proteins.

	WPD	α3	α6	α7
Apo PTP1B	1.66 ± 0.4	1.27 ± 0.13	1.05 ± 0.2	2.4 ± 0.34
BB2–PTP1B	1.30 ± 0.32	1.06 ± 0.32	0.9 ± 0.15	2.55 ± 0.29
Apo TCPTP	1.67 ± 0.29	1.31 ± 0.18	1.27 ± 0.13	5.16 ± 0.33
BB2–TCPTP	1.53 ± 0.46	1.36 ± 0.32	1.22 ± 0.24	2.70 ± 0.4

Stabilisation effects on the binding site were also studied in terms of protein–ligand contacts and concurrences. Ligand BB2 was able to establish up to 11 different contacts with neighbouring residues in PTP1B, namely, Glu276, Gly277, Lys279, Phe280, Ile281, Gly283, Ser285, Val287, Gln288, Trp291 and Lys292. In the case of the BB2–TCPTP complex, ligand contacts with up to 10 different residues during the MD simulation, namely, Glu274, Gly275, Lys277, Cys278, Ile279, Gly281, Ile285, Gln286, Trp289 and

Lys290.

In addition to the RMSD values for the WPD loop and allosteric helixes, the distance between the Cα of $Asp181_{PTP1B}$/$Asp182_{TCPTP}$ residue present in the WPD and the Cα of Ser216/ Ser217 for PTP1B/TCPTP, respectively, was calculated to assess changes in the conformation of the catalytic site (Fig. 6). As expected, distance between those atoms is, in general, well maintained for the apo proteins during simulation in the open sate. Only apo PTP1B showed distance increments at the beginning of the simulation because of WPD loop flipping for about 10 ns. In the case of ligand bound systems, average distances of 11.64 ± 0.61 and 11.93 ± 1.01 Å for BB2–PTP1B and BB2–TCPTP were respectively observed, suggesting a more mobile loop for the latter. Moreover, when the distance across the simulation time is represented, a significant ($p = 0.0001$) increment of up to 14.6 Å for the distance between those Cα is observed for BB2-TCPTP during the first 20 ns of simulation. This behaviour may be understood as the response exerted by the binding of BB2 on the whole protein, which undergoes slightly higher motions in the WPD loop, reflecting a weaker stabilisation of the inactive (open) form. As shown in Fig 6. C) WPD loop distance fluctuation (in terms of values distribution) is slightly lowered when BB2 is bound to PTP1B, while the opposite behaviour is observed for TCPTP. This may illustrate a greater stabilization effect of BB2 on PTP1B WPD loop.

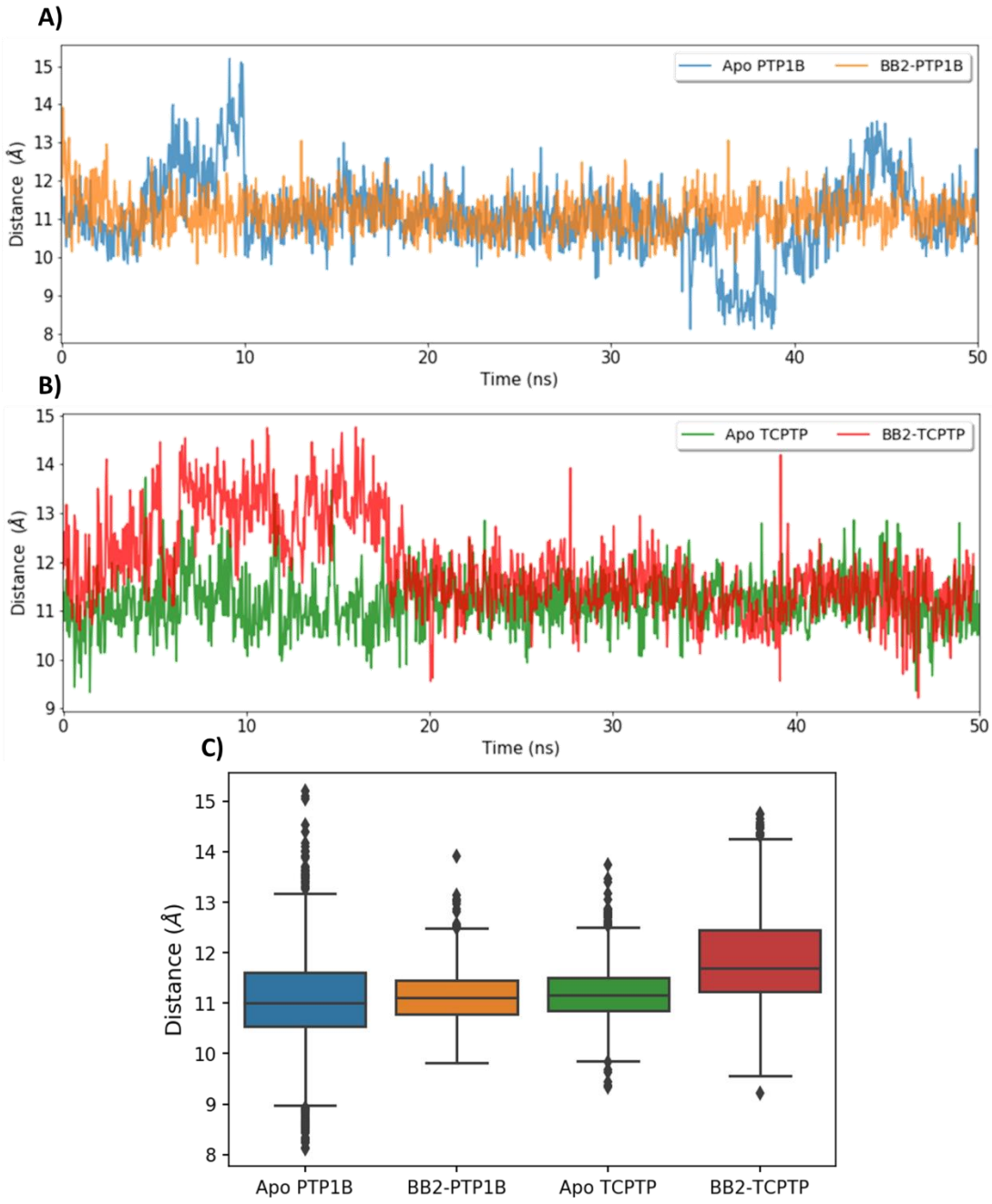

Fig. 6. A) Distances between the Cα of Asp181$_{PTP1B}$ and Cα of Ser216$_{PTP1B}$ present in the WPD. B) Distances between the Cα of Asp182$_{TCPTP}$ and Cα Ser217$_{TCPTP}$ present in the WPD. C) Box plots of WPD loop distances represented in A) and B).

To highlight the differences of WPD loop mobility, PCA was performed for the Cα of atoms comprising WPD loop of both complexes. This method allows to extract meaningful information from the complicated protein motions across the simulation. The Cartesian coordinate projections of the two principal components allowed to identify the most populated microstates for both enzymes. Since the time scale of this work did not allow us to investigate a broad conformational space, transitions in WPD loop between the open and closed conformations were not expected. Despite this, different ensembles were found for the open conformation of the WPD loop across the simulation. In the case of BB2–TCPTP, up to four different clusters of WPD loop were identified through the projection plot of PCA1 and PCA2 eigenvectors. In contrast, three better defined conformational states could be observed for BB2–PTP1B across the simulation (Fig. 7). These results demonstrate that the conformational distribution of WPD loop of TCPTP bound to BB2 was different from those bound to PTP1B. Furthermore, these analyses may illustrate the higher mobility of the WPD loop in BB2-TCPTP rather than BB2-PTP1B, allowing the exploration of novel conformational states.

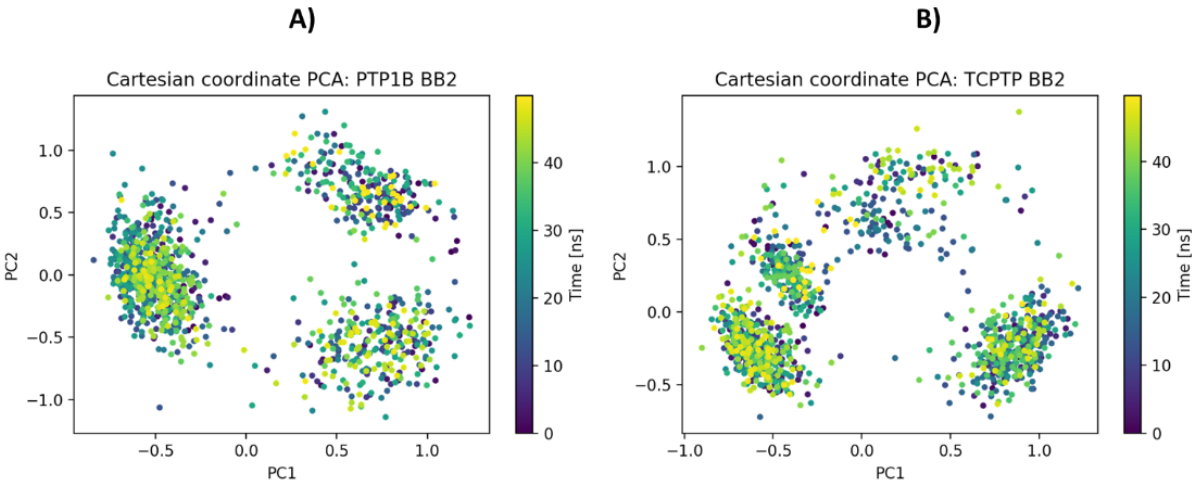

Fig. 7. Projection of the MD trajectories on their first two principal components for the Cα atoms comprising WPD loop of BB2–PTP1B (A) and BB2–TCPTP (B).

Free energy calculations

To get a deeper understanding of the selectivity between both enzymes, previous studies were also complemented with free energy calculations for BB2. As previously described, free energy calculations have been used for the study of selectivity between ligands and different or mutant targets (Fang, Wang, Xi, Liu, & Yin, 2016; Miller et al., 2012; Singh, Somvanshi, & Grover, 2019). Since the main differences in the allosteric site for both enzymes are Phe280/Cys278 and Val287/Ile285, we decided to study the contribution to free energy of these residues located inside the allosteric pocket. For this purpose, we took snapshots from the last 25 ns of MD, where the systems reached the equilibrium and the ligand remained more stable. Inhibitor BB2 showed a good energetic profile for both enzymes in accordance with a moderate binder, that is, -19.9275 ± 0.389 and -16.2504 ± 0.3387 kcal/mol for PTP1B and TCPTP, respectively. Further analysis of the energy terms revealed that electrostatic and intermolecular van der Waals interactions were favourable for binding, specially latter ones as previously described by other authors (Cui, W. et al., 2013; Kumar, R., Shinde, Ajay, & Sobhia, 2010; Shinde & Sobhia, 2013). This fact is in accordance with the hydrogen bond pattern of the ligand and with the presence of hydrophobic and aromatic portions in the molecule. Despite that, currently, free energy calculation methods are not sufficiently reliable to predict ligand affinity with accuracy, they may provide an opportunity to rank ligands for the same targets (Wang, E. et al., 2019). Slight differences between the two targets could be observed, probing that BB2 presents a better affinity for PTP1B than TCPTP, which is in good agreement with experimental data difference (IC_{50}) thus validating this methodology to rank them.

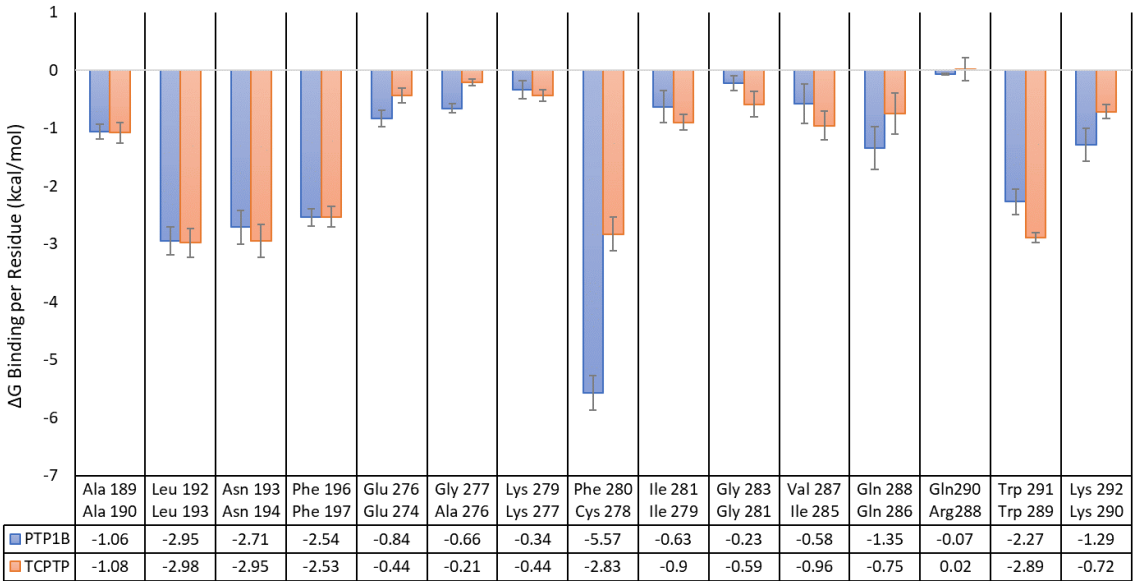

	Ala 189 Ala 190	Leu 192 Leu 193	Asn 193 Asn 194	Phe 196 Phe 197	Glu 276 Glu 274	Gly 277 Ala 276	Lys 279 Lys 277	Phe 280 Cys 278	Ile 281 Ile 279	Gly 283 Gly 281	Val 287 Ile 285	Gln 288 Gln 286	Gln290 Arg288	Trp 291 Trp 289	Lys 292 Lys 290
PTP1B	-1.06	-2.95	-2.71	-2.54	-0.84	-0.66	-0.34	-5.57	-0.63	-0.23	-0.58	-1.35	-0.07	-2.27	-1.29
TCPTP	-1.08	-2.98	-2.95	-2.53	-0.44	-0.21	-0.44	-2.83	-0.9	-0.59	-0.96	-0.75	0.02	-2.89	-0.72

Fig. 8. Per-residue free energy decomposition of BB2–PTP1B and BB2–TCPTP for the last 25 ns of simulation.

In 2013, Shinde *et al* hypothesised that the substitution of the Phe280 by Cys278 could play a key role in the selectivity over TCPTP (Shinde & Sobhia, 2013). To probe this hypothesis and to gain further insights into the selectivity, per-residue energy decomposition of the MMPBSA energy has also been undertaken to identify key residues for ligand binding (Figure 8) in both enzymes.

We focused our attention to the neighbouring residues of BB2 at the allosteric site, shown in Figure 8. This analysis allowed to identify the 'hotspot' residues with ΔG > 2 kcal/mol in the interaction. As shown in the plot, the most important residue for the free energy in PTP1B was Phe280 (−5.57 kcal/mol). It is worth noticing that this residue presented higher value than Asn193 and Glu276, which contribute to the binding mode through hydrogen bonds. This fact highlights the importance of hydrophobic and aromatic interactions for ligands in this kind of pocket, as previously observed, compared with electrostatic interactions (Cui, W. et al., 2013; Wang, Q., Fu, & Zheng, 2019). A very

different scenario is observed for TCPTP complex, where the highest contribution is given by Leu193 with −2.98 kcal/mol. The Cys278, which is placed at the same position as Phe280 in PTP1B, only contributes with −2.83 kcal/mol. This fact could be explained by the loss of the strong parallel π stacking by a much weaker hydrophobic interaction mediated by the side chain of Cys278. Other different residues in both proteins including Gln290$_{PTP1B}$/Arg288$_{TCPTP}$ did not significantly affect the free energy, probably because of its positioning in the highly mobile *C*-terminal part of the α7 helix. Compared with Val287$_{PTP1B}$, the Ile285$_{TCPTP}$ appeared to improve binding energy because of the van der Waals interactions that are established between the side chain of the residue and the benzofuran core/ethyl group of BB2. The residues Trp289$_{PTP1B}$/Trp290$_{TCPTP}$ also present a great contribution in both systems because of its π stacking with the benzofuran core. Surprisingly, the residues Glu276$_{PTP1B}$/Glu274$_{TCPTP}$ contributed poorly to the free energy. This could be explained by the proximity of the benzene ring in the sulphanilamide moiety of BB2, which is hydrophobic and has an unfavourable desolvation (Shinde & Sobhia, 2013).

Conclusion

In this study, models of the binary PTP1B-BB2 and TCPTP-BB2 complexes, together with the apoenzyme were generated and investigated using conventional MD and end-point free energy methods to rationalise and shed some light into its selectivity. To perform our analysis, homology models were created for the apo and ligand bound systems to obtain reliable whole structures. Then, MD showed that both systems are stable; however, especially for those bound to BB2, small differences could be observed during the simulation. This work identifies and highlights that allosteric site of the TCPTP

presented higher mobility and overall flexibility than that of PTP1B. This was also illustrated by the fluctuations of the ligand BB2 inside the pocket.

This study illustrates the crucial role that Phe280 plays in the allosteric recognition of PTP1B. Hydrophobic interactions, especially sandwich π stacking, could be an essential feature for the design of effective allosteric inhibitors of PTP1B, in terms of not only free energy but also stability of the final ligand–protein complex. In conclusion, this study provides significant insights into the allosteric recognition of benzbromarone derivatives and PTP1B. This better understanding could guide the design of new allosteric and selective inhibitors of PTP1B.

Conflict of interest

Author declared the is not any conflict of interest to publish this manuscript in Journal of Biomolecular Structure and Dynamics.

Funding

This work was supported by Ministerio de Economía y Competitividad (CTQ2017-85263-R) and Instituto de Salud Carlos III/REDinRED (RD16/0009/0015). Author is grateful for the Fellowships provided by University of Alcala and Ministerio de Educación Cultura y Deporte (FPU16/01647).

Acknowledgements

Author is grateful to Ramón Alajarín for its fruitful and invaluable conversation and manuscript supervision and J. J. Vaquero for its guidance. The author would like to thank Enago (www.enago.com) for the English language review. Author acknowledges Águeda Molinero-Fernández by its help with statistical analysis. Author is grateful to the anonymous reviewers for helpful suggestions.

References

Abdel-Magid, A. (2015). Allosteric modulators: An emerging concept in drug discovery. *ACS Medicinal Chemistry Letters, 6*(2), 104-107. doi:10.1021/ml5005365

Bence, K. K., Delibegovic, M., Xue, B., Gorgun, C. Z., Hotamisligil, G. S., Neel, B. G., & Kahn, B. B. (2006). Neuronal PTP1B regulates body weight, adiposity and leptin action. *Nature Medicine, 12*(8), 917-924. doi:10.1038/nm1435

Bharatham, K., Bharatham, N., Kwon, Y. J., & Lee, K. W. (2008). Molecular dynamics simulation study of PTP1B with allosteric inhibitor and its application in receptor based pharmacophore modeling. *Journal of Computer-Aided Molecular Design, 22*(12), 925. doi:10.1007/s10822-008-9229-0

Case, D. A., Cheatham III, T. E., Darden, T., Gohlke, H., Luo, R., Merz Jr., K. M., . . . Woods, R. J. (2005). The amber biomolecular simulation programs. *Journal of Computational Chemistry, 26*(16), 1668-1688. doi:10.1002/jcc.20290

Chatterjee, S., Khunti, K., & Davies, M. J. (2017). *Type 2 diabetes* doi:10.1016/S0140-6736(17)30058-2

Colombano, G., Caldwell, J. J., Matthews, T. P., Bhatia, C., Joshi, A., McHardy, T., . . . Collins, I. (2019). Binding to an unusual inactive kinase conformation by highly selective inhibitors of inositol-requiring enzyme 1α kinase-endoribonuclease. *Journal of Medicinal Chemistry, 62*(5), 2447-2465. doi:10.1021/acs.jmedchem.8b01721

Cui, D. S., Lipchock, J. M., Brookner, D., & Loria, J. P. (2019). Uncovering the molecular interactions in the catalytic loop that modulate the conformational dynamics in protein tyrosine phosphatase 1B. *Journal of the American Chemical Society, 141*(32), 12634-12647. doi:10.1021/jacs.9b04470

Cui, W., Cheng, Y., Geng, L., Liang, D., Hou, T., & Ji, M. (2013). Unraveling the allosteric inhibition mechanism of PTP1B by free energy calculation based on umbrella sampling. *Journal of Chemical Information and Modeling, 53*(5), 1157-1167. doi:10.1021/ci300526u

Elchebly, M., Payette, P., Michaliszyn, E., Cromlish, W., Collins, S., Loy, A. L., . . . Kennedy, B. P. (1999). Increased insulin sensitivity and obesity resistance in mice lacking the protein tyrosine phosphatase-1B gene. *Science (New York, N.Y.), 283*(5407), 1544-1548. doi:10.1126/science.283.5407.1544

Fang, L., Wang, X., Xi, M., Liu, T., & Yin, D. (2016). Assessing the ligand selectivity of sphingosine kinases using molecular dynamics and MM-PBSA binding free energy calculations. *Molecular bioSystems, 12*(4), 1174-1182. doi:10.1039/C6MB00067C

Garuti, L., & Bottegoni, M. Roberti and G. (2010). *Non-ATP competitive protein kinase inhibitors* doi:10.2174/092986710791859333

Genheden, S., & Ryde, U. (2010). How to obtain statistically converged MM/GBSA results. *Journal of Computational Chemistry, 31*(4), 837-846. doi:10.1002/jcc.21366

Huggins, D. J., Sherman, W., & Tidor, B. (2012). Rational approaches to improving selectivity in drug design. *Journal of Medicinal Chemistry, 55*(4), 1424-1444. doi:10.1021/jm2010332

Humphrey, W., Dalke, A., & Schulten, K. (1996). *VMD: Visual molecular dynamics* doi:10.1016/0263-7855(96)00018-5

Ito, M., Fukuda, S., Sakata, S., Morinaga, H., & Ohta, T. (2014). Pharmacological effects of JTT-551, a novel protein tyrosine phosphatase 1B inhibitor, in diet-induced obesity mice. *Journal of Diabetes Research, 2014* doi:10.1155/2014/680348

Jin, T., Yu, H., & Huang, X. (2016). Selective binding modes and allosteric inhibitory effects of lupane triterpenes on protein tyrosine phosphatase 1B. *Scientific Reports, 6*(1), 20766. doi:10.1038/srep20766

Johnson, T. O., Ermolieff, J., & Jirousek, M. R. (2002). Protein tyrosine phosphatase 1B inhibitors for diabetes. *Nature Reviews Drug Discovery, 1*(9), 696-709. doi:10.1038/nrd895

Jorgensen, W. L., Chandrasekhar, J., Madura, J. D., Impey, R. W., & Klein, M. L. (1983). Comparison of simple potential functions for simulating liquid water. *The Journal of Chemical Physics, 79*(2), 926-935. doi:10.1063/1.445869

Joyce, C. M., Potapova, O., DeLucia, A. M., Huang, X., Basu, V. P., & Grindley, N. D. F. (2008). Fingers-closing and other rapid conformational changes in DNA polymerase I (klenow fragment) and their role in nucleotide selectivity. *Biochemistry, 47*(23), 6103-6116. doi:10.1021/bi7021848

Kamerlin, S. C. L., Rucker, R., & Boresch, S. (2007). *A molecular dynamics study of WPD-loop flexibility in PTP1B* doi:10.1016/j.bbrc.2007.03.093

Kulkarni, Y. S., Liao, Q., Petrović, D., Krüger, D. M., Strodel, B., Amyes, T. L., . . . Kamerlin, S. C. L. (2017). Enzyme architecture: Modeling the operation of a hydrophobic clamp in catalysis by triosephosphate isomerase. *Journal of the American Chemical Society, 139*(30), 10514-10525. doi:10.1021/jacs.7b05576

Kumar, A. P., Nguyen, M. N., Verma, C., & Lukman, S. (2018). Structural analysis of protein tyrosine phosphatase 1B reveals potentially druggable allosteric binding sites. *Proteins: Structure, Function, and Bioinformatics, 86*(3), 301-321. doi:10.1002/prot.25440

Kumar, R., Shinde, R. N., Ajay, D., & Sobhia, M. E. (2010). Probing interaction requirements in PTP1B inhibitors: A comparative molecular dynamics study.

Journal of Chemical Information and Modeling, 50(6), 1147-1158. doi:10.1021/ci900484g

Li, S., Zhang, J., Lu, S., Huang, W., Geng, L., Shen, Q., & Zhang, J. (2014). The mechanism of allosteric inhibition of protein tyrosine phosphatase 1B. *PloS One, 9*(5), e97668. doi:10.1371/journal.pone.0097668

Maier, J. A., Martinez, C., Kasavajhala, K., Wickstrom, L., Hauser, K. E., & Simmerling, C. (2015). ff14SB: Improving the accuracy of protein side chain and backbone parameters from ff99SB. *Journal of Chemical Theory and Computation, 11*(8), 3696-3713. doi:10.1021/acs.jctc.5b00255

McGibbon, R., Beauchamp, K., Harrigan, M., Klein, C., Swails, J., Hernández, C., . . . Pande, V. (2015). *MDTraj: A modern open library for the analysis of molecular dynamics trajectories* doi:10.1016/j.bpj.2015.08.015

Miller, B. R., McGee, T. D., Swails, J. M., Homeyer, N., Gohlke, H., & Roitberg, A. E. (2012). MMPBSA.py: An efficient program for end-state free energy calculations. *Journal of Chemical Theory and Computation, 8*(9), 3314-3321. doi:10.1021/ct300418h

N K Tonks, C D Diltz, & E H Fischer. (1988). Purification of the major protein-tyrosine-phosphatases of human placenta. *Journal of Biological Chemistry, 263*(14), 6722. Retrieved from http://www.jbc.org/content/263/14/6722.abstract

Nosé, S. (1984). A unified formulation of the constant temperature molecular dynamics methods. *The Journal of Chemical Physics, 81*(1), 511-519. doi:10.1063/1.447334

Nussinov, R., & Tsai, C. J. (2013). Allostery in disease and in drug discovery. *Cell, 153*(2), 293-305. doi:S0092-8674(13)00391-7 [pii]

Olmez, E. O., & Alakent, B. (2011a). Alpha7 helix plays an important role in the conformational stability of PTP1B. *Journal of Biomolecular Structure and Dynamics, 28*(5), 675-693. doi:10.1080/07391102.2011.10508599

Olmez, E. O., & Alakent, B. (2011b). Alpha7 helix plays an important role in the conformational stability of PTP1B. *Journal of Biomolecular Structure and Dynamics, 28*(5), 675-693. doi:10.1080/07391102.2011.10508599

Pettersen, E. F., Goddard, T. D., Huang, C. C., Couch, G. S., Greenblatt, D. M., Meng, E. C., & Ferrin, T. E. (2004). UCSF Chimera—A visualization system for exploratory research and analysis. *Journal of Computational Chemistry, 25*(13), 1605-1612. doi:10.1002/jcc.20084

Phillips, J. C., Braun, R., Wang, W., Gumbart, J., Tajkhorshid, E., Villa, E., . . . Schulten, K. (2005). Scalable molecular dynamics with NAMD. *Journal of Computational Chemistry, 26*(16), 1781-1802. doi:10.1002/jcc.20289

Puius, Y. A., Zhao, Y., Sullivan, M., Lawrence, D. S., Almo, S. C., & Zhang, Z. Y. (1997). Identification of a second aryl phosphate-binding site in protein-tyrosine phosphatase 1B: A paradigm for inhibitor design. *Proceedings of the National Academy of Sciences of the United States of America, 94*(25), 13420-13425. doi:1813 [pii]

Raza, S., Ranaghan, K. E., van der Kamp, Marc W, Woods, C. J., Mulholland, A. J., & Azam, S. S. (2019). Visualizing protein-ligand binding with chemical energy-wise decomposition (CHEWD): Application to ligand binding in the kallikrein-8 S1 site. *Journal of Computer-Aided Molecular Design, 33*(5), 461-475. doi:10.1007/s10822-019-00200-4

Šali, A., & Blundell, T. L. (1993). *Comparative protein modelling by satisfaction of spatial restraints* doi:10.1006/jmbi.1993.1626

Shen, W., Erlanson, D. A., Taylor, L., Randal, M., Kung, J., Fahr, B. J., . . . Barr, K. J. (2004). Allosteric inhibition of protein tyrosine phosphatase 1B. *Nature Structural & Molecular Biology, 11*(8), 730-737. doi:10.1038/nsmb803

Shinde, R. N., Kumar, G. S., Eqbal, S., & Sobhia, M. E. (2018). Screening and identification of potential PTP1B allosteric inhibitors using in silico and in vitro approaches. *PloS One, 13*(6), e0199020. doi:10.1371/journal.pone.0199020

Shinde, R. N., & Sobhia, M. E. (2013). *Binding and discerning interactions of PTP1B allosteric inhibitors: Novel insights from molecular dynamics simulations* doi:10.1016/j.jmgm.2013.08.001

Singh, A., Somvanshi, P., & Grover, A. (2019). Pyrazinamide drug resistance in RpsA mutant (Δ438A) of mycobacterium tuberculosis: Dynamics of essential motions and free-energy landscape analysis. *Journal of Cellular Biochemistry, 120*(5), 7386-7402. doi:10.1002/jcb.28013

van Gunsteren, W. F., & Berendsen, H. J. C. (1977). Algorithms for macromolecular dynamics and constraint dynamics. *Molecular Physics, 34*(5), 1311-1327. doi:10.1080/00268977700102571

Wang, E., Sun, H., Wang, J., Wang, Z., Liu, H., Zhang, J. Z. H., & Hou, T. (2019). End-point binding free energy calculation with MM/PBSA and MM/GBSA: Strategies and applications in drug design. *Chemical Reviews, 119*(16), 9478-9508. doi:10.1021/acs.chemrev.9b00055

Wang, J., Wolf, R. M., Caldwell, J. W., Kollman, P. A., & Case, D. A. (2004). Development and testing of a general amber force field. *Journal of Computational Chemistry, 25*(9), 1157-1174. doi:10.1002/jcc.20035

Wang, Q., Fu, X., & Zheng, Q. (2019). Exploring the allosteric mechanism of protein tyrosine phosphatase 1B by molecular dynamics simulations. *Journal of Biomolecular Structure and Dynamics*, , 1-11. doi:10.1080/07391102.2019.1682049

Wiesmann, C., Barr, K. J., Kung, J., Zhu, J., Erlanson, D. A., Shen, W., . . . Hansen, S. K. (2004). Allosteric inhibition of protein tyrosine phosphatase 1B. *Nature Structural and Molecular Biology*, *11*(8), 730-737. doi:10.1038/nsmb803

Yangmee Kim, Jee-Young Lee, Ki-Woong Jung, & Eun-Rhan Woo. (2008). Docking study of biflavonoids, allosteric inhibitors of protein tyrosine phosphatase 1B. *Bulletin of the Korean Chemical Society*, *29*(8), 1479-1484. doi:10.5012/bkcs.2008.29.8.1479

You-Ten, K. E., Muise, E. S., Itié, A., Michaliszyn, E., Wagner, J., Jothy, S., . . . Tremblay, M. L. (1997). Impaired bone marrow microenvironment and immune function in T cell protein tyrosine phosphatase-deficient mice. *Journal of Experimental Medicine*, *186*(5), 683-693. doi:10.1084/jem.186.5.683

Zheng, Y., Ley, S. H., & Hu, F. B. (2018). Global aetiology and epidemiology of type 2 diabetes mellitus and its complications. *Nature Reviews. Endocrinology*, *14*(2), 88-98. doi:10.1038/nrendo.2017.151